Biomaterials Science

Electroactive polymer-peptide conjugates for adhesive biointerfaces

Journal:	*Biomaterials Science*
Manuscript ID:	BM-ART-05-2015-000160.R2
Article Type:	Paper
Date Submitted by the Author:	20-Jun-2015

Complete List of Authors:	Maione, Silvana; Universitat Politècnica de Catalunya, Gil, Ana; ISQCH, CSIC-Universidad de Zaragoza, Departamento de Química Orgánica Fabregat, Georgina; Universitat Politècnica de Catalunya, del Valle, Luis; Universitat Politècnica de Catalunya, Triguero Enguinados, Jordi; UPC, Chemical Engineering Laurent, Adèle; Université de Nantes, CEISAM UMR 6230 Jacquemin, Denis; Université de Nantes, CEISAM - UMR 6230 Estrany, Francesc; Universitat Politècnica de Catalunya, Jimenez, Ana; ISQCH, CSIC-Universidad de Zaragoza, Departamento de Química Orgánica Zanuy, David; UPC, Chemical Engineering Cativiela, Carlos; ISQCH, CSIC-Universidad de Zaragoza, Departamento de Química Orgánica Aleman, Carlos; Universitat Politecnica de Catalunya,

Journal Name

ARTICLE

Electroactive polymer-peptide conjugates for adhesive biointerfaces

Received 00th January 20xx,
Accepted 00th January 20xx

DOI: 10.1039/x0xx00000x

www.rsc.org/

Silvana Maione,[a,b] Ana M. Gil,[c] Georgina Fabregat,[a,b] Luis J. del Valle,[a,b] Jordi Triguero,[a] Adele Laurent,[d,e] Denis Jacquemin,[d,e] Francesc Estrany,[b,f] Ana I. Jiménez,[c] David Zanuy,[a] Carlos Cativiela[c,*] and Carlos Alemán[a,b,*c]

Electroactive polymer-peptide conjugates have been synthesized by combining poly(3,4-ethylenedioxythiophene), a polythiophene derivative with outstanding properties, and an Arg-Gly-Asp (RGD)-based peptide in which Gly has been replaced by an exotic amino acid bearing a 3,4-ethylenedioxythiophene ring in the side chain. The incorporation of the peptide at the end of preformed PEDOT chains has been corroborated by both FTIR and X-ray photoelectron spectroscopies. Although the morphology and topology are not influenced by the incorporation of the peptide to the end of PEDOT chains, this process largely affects other surface properties. Thus, the wettability of the conjugates is considerably higher than that of PEDOT, independently of the synthetic strategy, whereas the surface roughness only increases when the conjugate is obtained using a competing strategy (*i.e.* growth of the polymer chains against termination by end capping). The electrochemical activity of the conjugates has been found to be higher than that of PEDOT, evidencing the success of the polymer-peptide links designed by chemical similarity. Density Functional Theory calculations have been used not only to ascertain the conformational preferences of the peptide but also to interpret the electronic transitions detected by UV-vis spectroscopy. Electroactive surfaces prepared using the conjugates displayed the higher bioactivies in terms of cell adhesion, with the relative viabilities being dependent on the roughness, wettability and electrochemical activity of the conjugate. In addition to the influence of the peptide fragment in the initial cell attachment and subsequent cell spreading and survival, results indicate that PEDOT promotes the exchange of ions at the conjugate–cell interface.

Introduction

The RGD (Arg-Gly-Asp) amino acid sequence is the unit of a cell adhesive activity domain in adherent proteins (*e.g.* fibronectin, fibrin and vitronectin).[1-3] This cell adhesion motif has been widely used in the development of synthetic materials for bioengineering, different approaches being applied for such purpose (*e.g.* integration in larger peptide sequences,[4-7] surface functionalized substrates[8-12] and polymer-peptide conjugates[12-15]). In all cases RGD-containing biomaterials increased the cellular adhesion with respect to the control when the adhesion motif was immobilized maintaining its biological activity.

Among advanced organic biomaterials, polymer-peptide conjugates, which result from the covalent integration of a peptide with a synthetic polymer block, are especially attractive because this kind of hybrid macromolecules combines unique properties that come from the precise chemical structure and functionality of peptides and the stability, functions and processability of synthetic polymers.[16-19] In order to take advantage of the electrochemical properties of electroactive conducting polymers (ECPs), different ECP-peptide conjugates have been prepared during the last decade. For example, the first oligothiophene directly conjugated to a β-sheet pentapeptide was reported in 2004,[20] while the modification of the β-position on polypyrrole (PPy) to create strong disulfide bonds with the Cys of the RGDS sequence (Arg–Gly–Asp–Cys) was described in earlier works.[21,22] Within this context, we have recently reported a new strategy for the preparation of ECP-peptide conjugates that is based on the chemical similarity of their two components.[23,24] This approach is based on the design of exotic synthetic amino acids bearing the main chemical groups

[a] Departament d'Enginyeria Química, E. T. S. d'Enginyeria Industrial de Barcelona, Universitat Politècnica de Catalunya, Diagonal 647, 08028 Barcelona, Spain. E-mail: carlos.aleman@upc.edu
[b] Center for Research in Nano-Engineering, Universitat Politècnica de Catalunya, Campus Sud, Edifici C', C/Pasqual i Vila s/n, Barcelona E-08028, Spain.
[c] Departmento de Química Orgánica, Instituto de Síntesis Química y Catálisis Homogénea (ISQCH), University of Zaragoza–CSIC, 50009 Zaragoza, Spain. E-mail: cativiela@unizar.es
[d] CEISAM, UMR CNRS 6230, Faculté des Sciences et des Techniques, BP 92208, Université de Nantes, 2, rue de la Houssinière, 44322 Nantes Cedex ,France.
[e] Institut Universitaire de France, 103 bd St Michel, 75005 Paris Cedex 5, France.
[f] Departament d'Enginyeria Química, Escola Universitaria d'Enginyeria Tècnica Industrial de Barcelona, Universitat Politècnica de Catalunya, Comte d'Urgell 187, 08036 Barcelona, Spain

† Electronic Supplementary Information (ESI) available: synthetic intermediates, characterization methods, XPS spectra, SEM and AFM micrographs, cyclic voltammograms and plots of the electron density difference. See DOI: 10.1039/x0xx00000x

of the polymer to facilitate the covalent conjugation between the components. Such methodology avoids the presence of long aliphatic linkers, which are typically used to join the two components of the polymer-peptide conjugate. The absence of linkers is expected to promote the extension of the polymer properties towards the peptide surface region, which is an important limitation typically found in ECP-peptide conjugates.

In this work we have used a strategy based on chemical similarity to design an electroactive RGD-based ECP-peptide conjugate. The polymer selected for this purpose is poly(3,4-ethylenedioxythiophene), hereafter abbreviated PEDOT, which is among the most successful ECPs due to its excellent electrochemical and thermal properties, high conductivity, good environmental stability in its doped state, mechanical flexibility, relative ease of preparation, and fast doping-undoping process.[25-27] Regarding to the peptide, the Gly residue of the RGD sequence has been replaced by GlE, which consists of an amino acid bearing a 3,4-ethylenedioxythiophene as side group attached to an additional methylene group. The resulting sequence, hereafter denoted RG^{E}D, has been attached to end of PEDOT chains forming the PEDOT-RG^{E}D conjugate (Scheme 1). After chemical characterization, the physical properties of the conjugate have been investigated at different length scales. Finally, benefits induced by conjugation in tissue regeneration have been investigated by comparing the behavior of PEDOT and PEDOT-RG^{E}D as soft bioelectroactive supports for cell attachment.

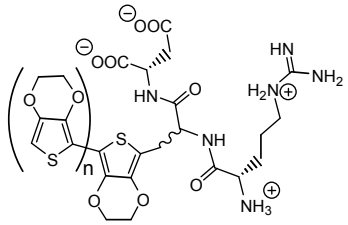

PEDOT-RG^{E}D

Scheme 1. Chemical structure of the PEDOT-RG^{E}D conjugate

Results and discussion

Synthesis of the protected RG^{E}D peptide

The synthetic route used to obtain the RG^{E}D sequence, which was protected at the reactive positions by *tert*-butyl ester groups (^{t}Bu-COO) to avoid interferences during the coupling to PEDOT chains, is provided in Figure 1.

Preparation and chemical characterization of the **1-5** intermediates is reported in the Electronic Supporting Information (ESI). The procedure used to prepare the protected RG^{E}D peptide was as follows: To a solution of Boc-L-Arg(Boc)$_2$-OH (500 mg, 1.05 mmol) in dichloromethane (60 mL) cooled to 0 ºC in an ice bath, was added 1-hydroxybenzotriazole hydrate (HOBt) (161 mg, 1.05 mmol) and *N*-[3-(dimethylamino)-propyl]-*N'*-ethylcarbodiimide hydrochloride (EDC·HCl) (201 mg, 1.05 mmol) followed by a solution of H-D,L-GlE-Asp(O^{t}Bu)-O^{t}Bu (1 mmol) [obtained by deprotection of **5** (678 mg, 1 mmol) with diethylamine (DEA; 5 mL, 50 mmol)] in dichloromethane (10 mL) and finally *N*-methylmorpholine (NMM; 0.11 mL, 1 mmol). The reaction mixture was stirred at room temperature for 24 h. Then, the solution was washed with 5% $NaHCO_3$ (3×30 mL) followed by 5% $KHSO_4$ (3×30 mL). The organic phase was dried over magnesium sulfate and evaporated to dryness. The crude product was purified by column chromatography (eluent: hexane/ethyl acetate 6/4) to provide protected RG^{E}D (mixture of diastereoisomers) as a white solid (822 mg, 0.90 mmol, 90% yield).

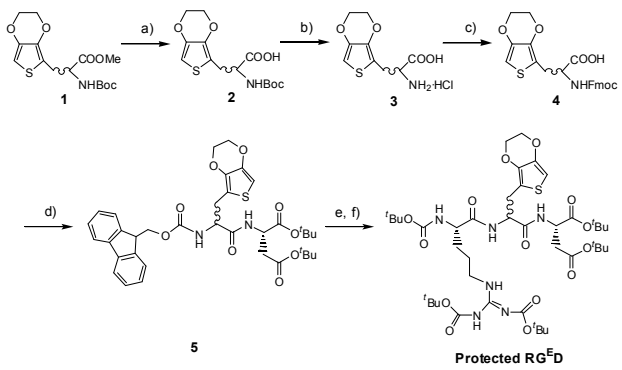

Figure 1. Reagents and conditions for the synthesis of protected RG^{E}D: (a) KOH 2N/MeOH, rt 2h, 99%; (b) HCl (3N)/AcOEt, rt 30 min, 100%; (c) FmocOsu, K_2CO_3, CH_3CN/H_2O 3/1, 80%; (d) HOBt, EDC·HCl, NMM, H-L-Asp(O^{t}Bu)-O^{t}Bu, CH_2Cl_2, 0ºC 30 min, rt 24h, 95%; (e) DEA, CH_2Cl_2, rt 4h, 100%; (f) HOBt, EDC·HCl, NMM, Boc-L-Arg(Boc)$_2$-OH, CH_2Cl_2, 0ºC 30 min, rt 24h, 90%.

IR (KBr) ν: 3381, 1715, 1610 cm^{-1}.^{1}H NMR ($CDCl_3$, 400 MHz): δ 1.37–1.85 (m, 4H), 1.43, 1.50, 1.51 (3s, 45H), 2.59–2.72 (m, 1H), 2.73–2.87 (m, 1H), 3.02–3.22 (m, 2H), 3.72–3.89 (m, 2H), 4.08–4.27 (m, 5H), 4.55–4.71 (m, 2H), 5.49–5.66 (m, 1H), 6.11, 6.12 (2s, 1H), 6.83–7.13 (m, 2H), 9.08–9.52 (m, 2H). ^{13}C NMR ($CDCl_3$, 125 MHz): δ 24.8, 24.9, 28.0, 28.18, 28.21, 28.4, 28.5, 28.8, 29.0, 29.8, 37.56, 37.59, 44.25, 44.29, 49.3, 49.5, 53.9, 54.0, 54.5, 54.7, 64.70, 64.72, 64.9, 79.1, 79.2, 81.5, 81.6, 82.29, 82.33, 84.0, 84.1, 97.3, 97.4, 111.26, 11.32, 139.3, 141.52, 141.54, 155.05, 155.08, 155.9, 160.7, 160.8, 163.71, 163.73, 169.4, 169.5, 169.92, 169.98, 170.1, 171.97, 172.22. HRMS (ESI) $C_{42}H_{69}N_6O_{14}S$ $[M+H]^+$: calcd. 913.4587, found 913.4609.

Synthesis of the PEDOT-RG^{E}D conjugate

The PEDOT-RG^{E}D conjugate was prepared using two alternative strategies (A and B) of three steps each one, which are known to provide materials with different surface properties.[28] In the first step, which is the same for the two strategies (Figure 2), PEDOT films were deposited onto steel sheets by chronoamperometry (CA) under a constant potential of 1.40 V and using a 10 mM 3,4-ethylenedioxythiophene (EDOT) solution in acetonitrile containing 100 mM $LiClO_4$ as supporting electrolyte. The polymerization time (θ_1) was only 10 s. After eliminating the excess of monomer and dopant from the prepared PEDOT films and washing with acetonitrile, the second step of each strategy was addressed (Figure 2).

Journal Name

ARTICLE

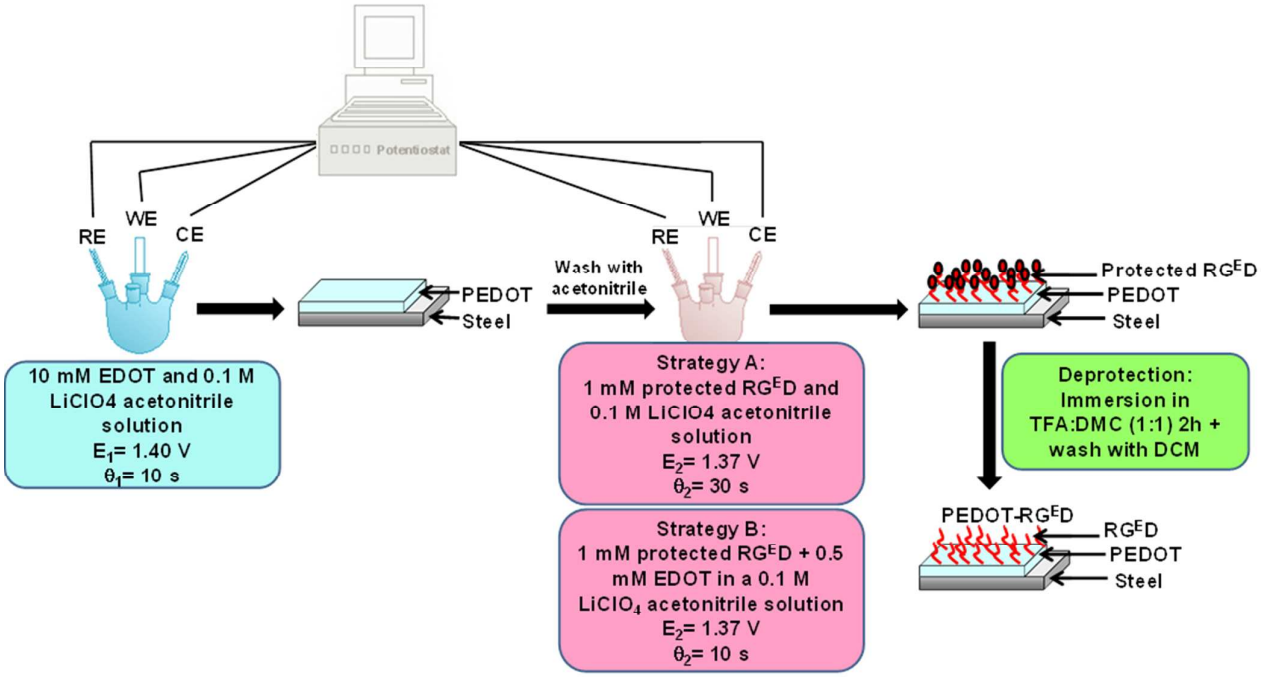

Figure 2. Scheme displaying the two synthetic strategies (A and B) used to prepare PEDOT-RG^{E}D. Each strategy involved a three-step process, even though A and B only differ in the conditions used for the intermediate step. RE, WE and CE refer to reference electrode, working electrode and counter electrode, respectively.

In strategy A, the electrode coated with the PEDOT was introduced in a cell containing an acetonitrile solution with 1 mM of protected RG^{E}D and 0.1 M $LiClO_4$, a constant potential of 1.37 V being applied during a time θ_2 = 30 s. In strategy B, the PEDOT film was introduced in a cell filled with a 1 mM RG^{E}D, 0.5 mM EDOT and 0.1 M $LiClO_4$ acetonitrile solution. In this case, a constant potential of 1.37 V was applied during θ_2 = 10 s only. Accordingly, the main differences between strategies A and B can be summarized as follow: (i) the generation medium used in B for the preparation of the conjugate contains both peptide and monomer in the second step, while that employed in A only contains peptide; and (ii) the polymerization time, θ_2, is significantly larger in A than in B. These modifications are expected to affect considerably the roughness and wettability of the surface.[28] Finally, in the last step, which was identical for strategies A and B (Figure 2), desired PEDOT-RG^{E}D conjugates were obtained by immersing electrodes coated with the PEDOT-(protected RG^{E}D) systems into a 1:1 trifluoacetic acid:dichloromethane mixture (TFA:DCM) by 2 hours and, subsequently, washing with DCM. Thus, this step was exclusively focused on the deprotection of the peptide fragments once they have been attached to the ECP chains. Hereafter, conjugates derived from strategies A and B have been labelled as PEDOT-RG^{E}D/A and PEDOT-RG^{E}D/B, respectively.

The average thickness, as determined by contact profilometry, of PEDOT-RG^{E}D/A and PEDOT-RG^{E}D/B films was 296±21 and 472±15 nm, respectively. On the other hand, PEDOT films used as a control during the whole work were prepared by immersing the films achieved in the first step into a cell containing an acetonitrile solution with 0.1 M $LiClO_4$ (*i.e.* without peptide and monomer) and applying a constant potential of 1.37 V during θ_2 = 10 s. This methodology allowed us to obtain ECP films with doping levels similar to that achieved for PEDOT-RG^{E}D/B. The average thickness of films derived from this process was 280±44 nm.

Comparison of the FTIR spectra of PEDOT, PEDOT-RG^{E}D/A and PEDOT-RG^{E}D/B (Figure 3) corroborates the incorporation of the RG^{E}D peptide. Thus, the amide II and amide III bands, which arise from the coupling between the N–H in-plane bending and C–N stretching modes, are clearly recognizable at approximately 1520 and 1320 cm^{-1}, respectively, for the two conjugates. Unfortunately, the Arg and Asp side chain bands at around 1620 and 1708 cm^{-1},[29] respectively, are not identified because of the overlapping with the associated to the thiophene ring (C=C and C–C stretching) of PEDOT.[23,30]

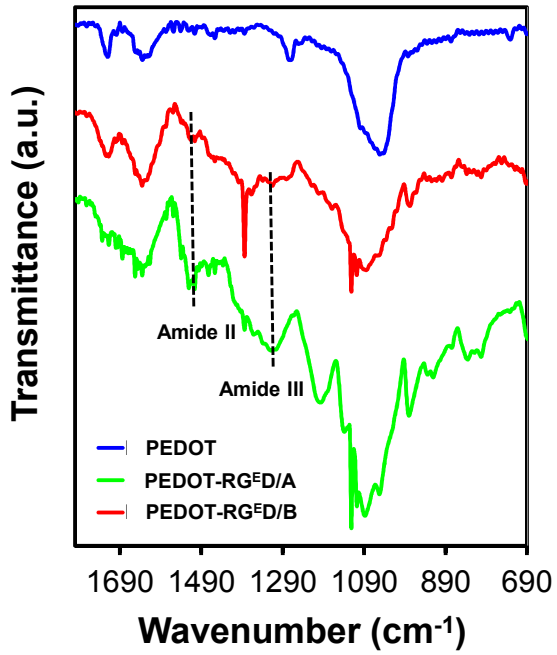

Figure 3. FTIR spectra of PEDOT, PEDOT-RG^{E}D/A and PEDOT-RG^{E}D/B.

The chemical structure of PEDOT-RG^{E}D films was further characterized by X-ray photoelectron spectroscopy (XPS). Table 1 compares the surface atomic compositions. The penetration of X-ray radiation using the conditions described in Methods section is expected to be ~10 nm, even though in this case the penetration is unknown because of both the nanometric thickness and porosity (next sub-section) of the films. This feature explains the detection of a small percentage of nitrogen in PEDOT samples, which cannot be attributed to traces of acetonitrile since samples were stored for almost two weeks before XPS analyses. Thus, detailed interpretation of the N1s (see below) allowed us to conclude that the nitrogen detected in the composition of PEDOT comes from the AISI 316 steel substrate. However, the N1s increases from 0.43% in PEDOT to 0.81% and 1.58% in PEDOT-RG^{E}D/A and PEDOT-RG^{E}D/B, respectively, supporting the successful incorporation of the peptide. For PEDOT, the C/S ratio, 6.22, is close to the theoretical value of 6.00, while such ratio increases to 6.90 and 7.20 for PEDOT-RG^{E}D/A and PEDOT-RG^{E}D/B, respectively. This observation is consistent with the fact that the increment of the content of C in the two conjugates is due to the incorporation of the RG^{E}D peptide.

Figures 4a-4d displays the high-resolution XPS spectrum in the C1s, N1s, O1s and S2p regions for PEDOT-RG^{E}D/B, the spectra for PEDOT-RG^{E}D/A being reported in the Figure S1. Before discussing the analysis, it should be mentioned that the peaks of the peptide may be influenced by those of PEDOT and vice versa, explaining the small deviations found in some peaks with respect to the values reported in the literature.

Deconvolution of the C1s peak led to five Gaussian curves that has been attributed to saturated and conjugated C–C (284.5 eV) and C=C–O (286.4 eV) bonds of PEDOT chains,[30,31] the C=O of amide (288.3 eV),[32,33] the C–N bonds of guanidinium group in Arg (289.6 eV)[33] and the C–F bonds of residual TFA molecules (292.2 eV)[33] arising from the deprotection step in the synthesis (Figure 2). The high resolution N1s spectrum shows a peak centered at 400.3 eV, which seems to include both the guanidinium (400.1 eV) and the backbone amide (400.6 eV) signals identified for the RGD peptide sequence.[33] The peak at 402.0 eV, which was also detected in PEDOT samples, has been attributed to impurities of the substrate.[23]

The O1s signal consists of three components, with the most intense one at 533.3 eV corresponding to the C–O–C bond in the ethylene bridge of PEDOT.[30] The component at 531.4 eV is assigned to the carboxylate groups in the conjugated RG^{E}D peptide[33] while the peak at 535.2 eV corresponds to the C=O of contamination products (*e.g.* CO_2 adsorbed from the atmosphere).[23,34] The latter is typically found in PEDOT produced by anodic polymerization and doped with lithium perchlorate.[23,34] The high resolution XPS of the S2p region of the conjugate shows the spin-split sulfur coupling $S2p_{3/2}$ and $S2p_{1/2}$, with a separation of 1.2 eV, for the C–S–C bond of the thiophene ring (163.9 and 165.1 eV, respectively) in PEDOT, its homologous with positively charged sulfur (*i.e.* C–S^+–C 165.5 and 166.7 eV, respectively), and the C–S–C bond of the side chain of the GlE residue in the peptide (at 167.8 and 169.0 eV, respectively).[35,36]

Table 1. Atomic percent composition (C1s, O1s, N1s, S2p and Cl2p) obtained by XPS for PEDOT, PEDOT-RG^{E}D/A and PEDOT-RG^{E}D/B samples.

	C1s	N1s	O1s	S2p	Cl2p
PEDOT	50.56	0.43	36.90	8.12	3.99
PEDOT+TFA	57.74	0.47	31.62	8.80	1.17
PEDOT-RG^{E}D/A	62.01	0.81	27.85	8.98	0.35
PEDOT-RG^{E}D/B	61.54	1.58	27.78	8.55	0.55

Spectra in the Cl2p regions for PEDOT-RG^{E}D/B and PEDOT-RG^{E}D/A show peaks at 207.6 and 209.2 eV (Figure S2), which correspond to the spin-split chloride coupling $Cl2p_{3/2}$ and $Cl2p_{1/2}$, with a separation of 1.6 eV, for the Cl–O bond of the perchlorate dopant agent. The Cl/S ratios obtained using the atomic percent compositions displayed in Table 1 have been directly associated to the doping level (DL), which corresponds to the number of positive charges per thiophene ring. The DL is very high for PEDOT, DL= +0.49, indicating that the formula of the ECP is: $[(EDOT^{0.49+})_n\ (ClO_4^-)_{0.49\cdot n}]_{solid}$. Very similar results (DL= +0.54) have been obtained by determining the amount of chloride with standard ion chromatography. In contrast, the DL of the two conjugates decreases to ~ +0.05, indicating a notable reduction of the salt structure behavior. In order to ascertain, one of the possible reasons of such drastic reduction, PEDOT films were immersed into a 1:1 TFA:DCM by 2 hours and, subsequently, washed with DCM, emulating the step used to eliminate the protection of peptide fragments in PEDOT-(protected RG^{E}D) systems. XPS analyses of the resulting films (PEDOT+TFA in Table 1) indicate that the DL of PEDOT decreases by from +0.49 to +0.13 upon treatment with TFA.

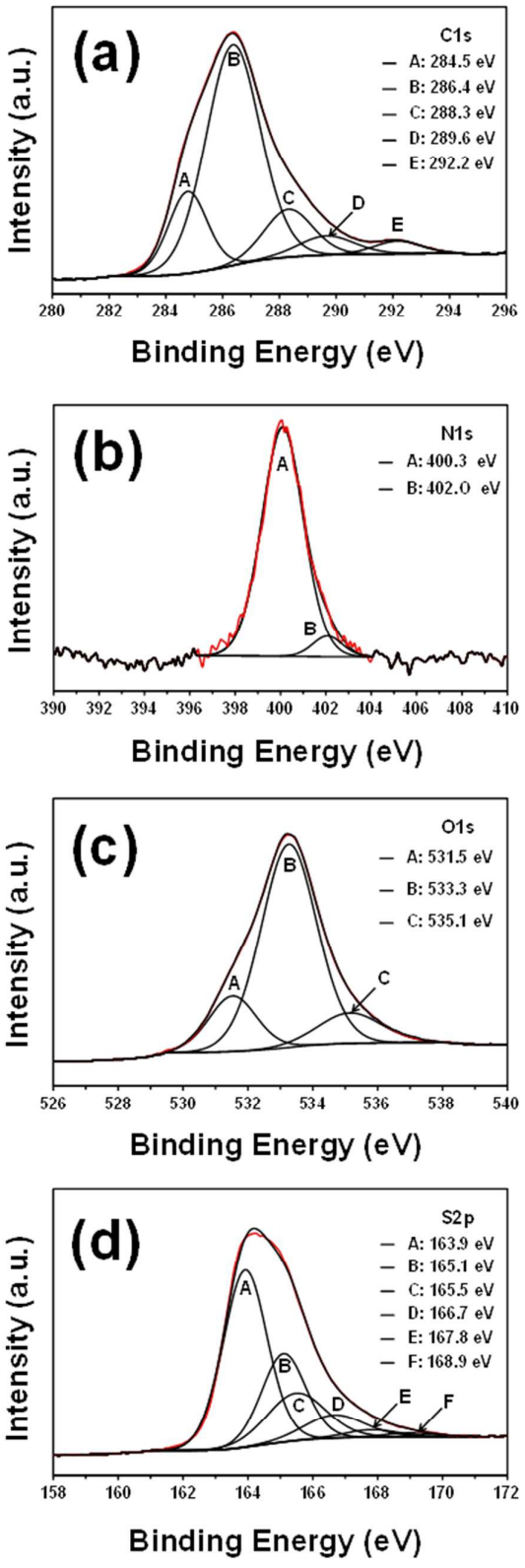

Figure 4. High-resolution XPS spectra for PEDOT-RG^{E}D/B: C1s (a), N1s (b), O1s (c) and S2p (d) regions. Peaks from deconvolution are also displayed. The red line corresponds to the experimental profile while the black line is the sum of the deconvoluted peaks.

Surface characterization

The surface morphology and topography of PEDOT-RG^{E}D conjugates were investigated using scanning electron microscopy (SEM) and atomic force microscopy (AFM), respectively. SEM micrographs of PEDOT-RG^{E}D/B (Figure 5a) indicate a structure formed by the aggregation of sticks with a fiber-like morphology, which facilitate the formation of narrow and tortuous pores. Comparison with micrographs obtained for PEDOT-RG^{E}D/A, as prepared PEDOT, and PEDOT treated with 1:1 TFA:DCM by 2 hours (Figure S3) indicates that the impact in the surface morphology of both end capping peptides and the applied deprotection treatment is practically negligible. Similarly, the surface topography of PEDOT-RG^{E}D/B (Figure 5b), that can be described as a dense and homogeneous distribution of sharp peaks grouped in clusters, is apparently indistinguishable from those of PEDOT and PEDOT-RG^{E}D/A (Figure S4). This topology, which is consequence of the linear growing of polymer chains (*i.e.* molecules are exclusively formed by α-α linkages because the β-positions of the thiophene ring are occupied by the dioxane ring),[37] is not altered by the incorporation of the RG^{E}D peptide at the ends.

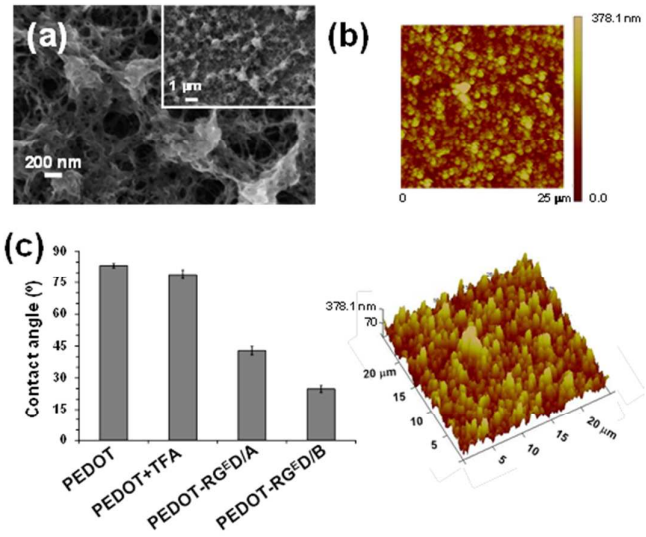

Figure 5. (a) SEM micrographs, high and low (inset) magnifications, and (b) 2D and 3D topographic images of PEDOT-RG^{E}D/B. (c) Contact angles of water (average and standard deviation of 14 independent measures) for as prepared PEDOT, PEDOT treated with 1:1 TFA:DCM by 2 hours and, subsequently, washed with DCM (PEDOT+TFA), emulating the step used to eliminate the protection of peptide fragments in PEDOT-(protected RG^{E}D) systems, and the two prepared conjugates.

In spite of their morphological similarity, the surface roughness of PEDOT-RG^{E}D conjugates has been found to depend on the approach used in the intermediate step of the synthetic process. Thus, the root-mean-square roughness (Rq) of PEDOT and PEDOT-RG^{E}D/A (Rq= 117±28 and 114±14 nm, respectively) are ~25% lower than that of PEDOT-RG^{E}D/B (Rq= 149±22 nm). This effect has been attributed to the coexistence and competition of two chemical processes in the intermediate step of strategy B: growth of polymer chains by

incorporating EDOT monomers and termination of polymer chains by incorporating RG^{E}D. In contrast, the termination was the only process present in strategy A. On the other, the thickness determined by AFM scratching tests using the tip in contact mode (Figure S5) was 350±10, 361±15 and 443±7 nm for PEDOT, PEDOT-RG^{E}D/A and PEDOT-RG^{E}D/B, respectively, these values being fully consistent with those obtained by contact profilometry.

The contact angles (Θ) measured in water (Figure 5c) indicate that PEDOT is a hydrophilic material (*i.e.* Θ < 90º), which should be attributed to the oxygen atoms of the fused dioxane ring. The wettability increases significantly upon the incorporation of RG^{E}D to the end of polymer chains, independently of the strategy used in the synthetic process (*i.e.* $\Delta\Theta$ > 40º in all cases). However, the effect of the synthetic strategy is not negligible, the contact angle of PEDOT-RG^{E}D/B being 18º lower than that of PEDOT-RG^{E}D/A. The increment of both wettability and Rq suggest that the conjugate derived from synthetic strategy B is more appropriated for tissue engineering applications than that produced using A. On the other hand, the contact angle determined for PEDOT treated with 1:1 TFA:DCM by 2 hours (Figure 5c) indicates that the end capping peptide is responsible of the remarkable wettability of two conjugates, the impact of the changes produced by the acid treatment being practically null ($\Delta\Theta\approx$ 4º).

Electroactivity and electrostability

Cyclic voltammetry (CV) studies were conducted to determine the influence of the end capping peptide in the electrochemical properties of the ECP. Control voltammograms recorded in phosphate buffered saline solution (PBS), which represents a physiological medium, are displayed in Figure 6a. The ability to exchange charge reversibly, hereafter denoted electroactivity, increases with the similarity between the anodic and cathodic areas of the control voltammogram. The electroactivity of PEDOT-RG^{E}D/A and PEDOT-RG^{E}D/B is, respectively, 57% and 75% higher than that of PEDOT. This feature points out the remarkable success of the strategy based on the design of ECP-peptide conjugates by chemical similarity. Thus, conjugation between the two components through a synthetic amino acid bearing the repeat unit of PEDOT as side chain rather than using long and flexible linkers, as is frequently done, facilitates the movement of charge from the bulk to the film-solution interface during the oxidation process (or from the interface to the bulk in the reduction process). Furthermore, charges located at ionized Arg and Asp residues, which are placed at the surface of film, also contribute to facilitate the access or escape of dopant ions during the redox processes. Consequently, the flow of ions is higher for PEDOT-RG^{E}D than for PEDOT. On the other hand, the ability to store charge is 11% higher for PEDOT-RG^{E}D/B than for PEDOT-RG^{E}D/A. This has been attributed to the accessibility of both PEDOT fragments and RG^{E}D peptides at the surface of films, which is promoted by synthetic strategy B (Figure 6b). These surface characteristics affect not only to the electroactivity, roughness and wettability but also to the electrochemical stability (electrostability).

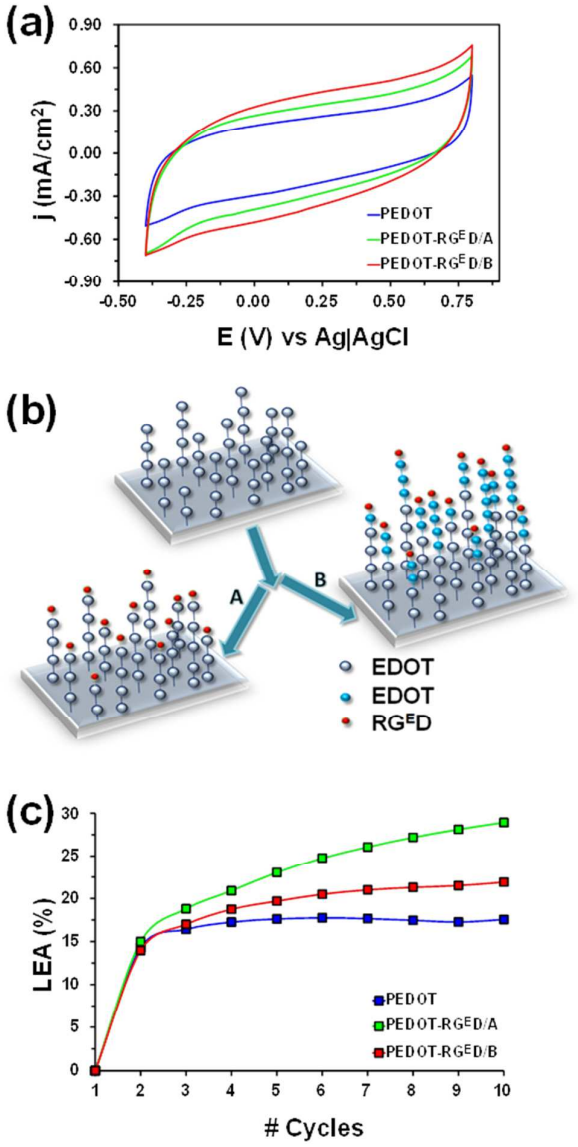

Figure 6. (a) Control voltammograms of PEDOT, PEDOT-RG^{E}D/A and PEDOT-RG^{E}D/B in PBS. Initial and final potentials, −0.40 V; reversal potential, 0.80 V; scan rate, 50 mV s_E^{-1}. (b) Scheme reflecting surface structural differences between PEDOT-RG^{E}D/A and PEDOT-RG^{E}D/B conjugates. (c) Loss of electroactivity (LEA) against the number of consecutive oxidation and reduction cycles in 0.1 M PBS for PEDOT, PEDOT-RG^{E}D/A and PEDOT-RG^{E}D/B.

The electrostability was evaluated by applying ten consecutive oxidation-reduction cycles in PBS. Figure 6c represents the loss of electroactivity (LEA) relative to the first cycle against the number of cycles. For PEDOT, the LEA stabilizes at 17% in the fourth cycle, reaching a plateau that reflects the high electrochemical stability of this ECP. In contrast, the LEA grows progressively with the number of cycles for PEDOT-RG^{E}D/A, the observed value after 10 cycles being LEA= 29%. PEDOT-RG^{E}D/B exhibits an intermediate behavior. Thus, the LEA slowly increases with the number of redox cycles (*i.e.* LEA=

22% after 10 cycles) and, simultaneously, tends to stabilize around a slightly higher value. According to these results, the conjugation of RG^ED has a negative effect in the electrochemical stability of PEDOT, which should be attributed to the degradation of the peptide during the oxidation and reduction processes. This undesirable effect is partially mitigated by the synthetic strategy B, which takes advantage of the excellent electrochemical properties of PEDOT (Figure 6b). Thus, negative effects on the electrostability caused by the peptide deterioration decrease with increasing surface reachability of PEDOT chains.

Molecular conformation and optical properties

The conformational potential energy surface of the RG^ED peptide was systematically explored using a procedure inspired in the build-up method early developed by Scheraga and coworkers[38] (see ESI). This method uses the geometries of smaller peptide segments to build the structures of larger segments. Accordingly, 559 starting conformations were constructed by combining the most stable minima identified for each of the involved residues. The geometry of all these structures was optimized at the B3LYP/6-31+G(d,p) level of theory in aqueous solution, solvent effects being modeled by the Polarizable Continuum Model (PCM). The resulting 552 minima were grouped in a list of 26 unique minimum energy conformations, which was constructed by assessing the similarities among the different structures (clustering of structures described in the Methods section). Figure 7a displays the distribution of such unique minima in the maps constructed using the backbone dihedral angles of Arg (ω,ψ), GlE (φ,ψ) and Asp (ω,φ) residues. As it can be seen, Arg and Asp tend to adopt an extended arrangement with ψ≈ 180º and φ≈ 180º, respectively, even though the latter also shows three minima with φ≈ 60º. Despite this apparent backbone homogeneity, both Arg and Asp present significant conformational variability at their side chains giving place to different networks of side chain···backbone interactions (Figure 7b). In contrast, the GlE residue exhibits remarkable conformational variability at the backone displaying minima in the α_R (φ,ψ≈ -70º,-20º), C_{7eq} (φ,ψ≈ -80º,80º) and β (φ,ψ≈ -150º, 60º) regions of the φ,ψ-map.

Figure 7b depicts the five unique minimum energy conformations with relative energy (ΔE) lower than 5 kcal/mol, which have labeled with letters A-E in increasing order of energy. The lowest energy minimum (A) is stabilized by a complex network of hydrogen bonds that include: (i) two backbone···backbone (b-b) interactions involving the ionized N- and C-terminal group and the C=O and N-H moieties of the adjacent amide groups (*i.e.* known as C_5 interactions because atoms involved in such known define a five-membered ring); (ii) one side chain····backbone (sc-b) salt bridge between the carboxylate side group of Asp and the ionized N-terminus; and (iii) one side chain···side chain (sc-sc) interaction between the guanidium group of Arg and the dioxane ring of GlE. In addition, this structure is stabilized by a N–H···π interaction between the guanidium group of Arg and the thiophene ring of GlE. Such interaction has not been identified in any other unique minimum with ΔE≤ 5 kcal/mol. The next minimum (B), which is practically isoenergetic to A (ΔE < 0.1 kcal/mol), exhibits the same b-b and sc-b interactions. Thus, the only difference between A and B refers to the sc-sc interaction that, in the latter, consists of a hydrogen bond between the guanidium group and the C=O of Arg.

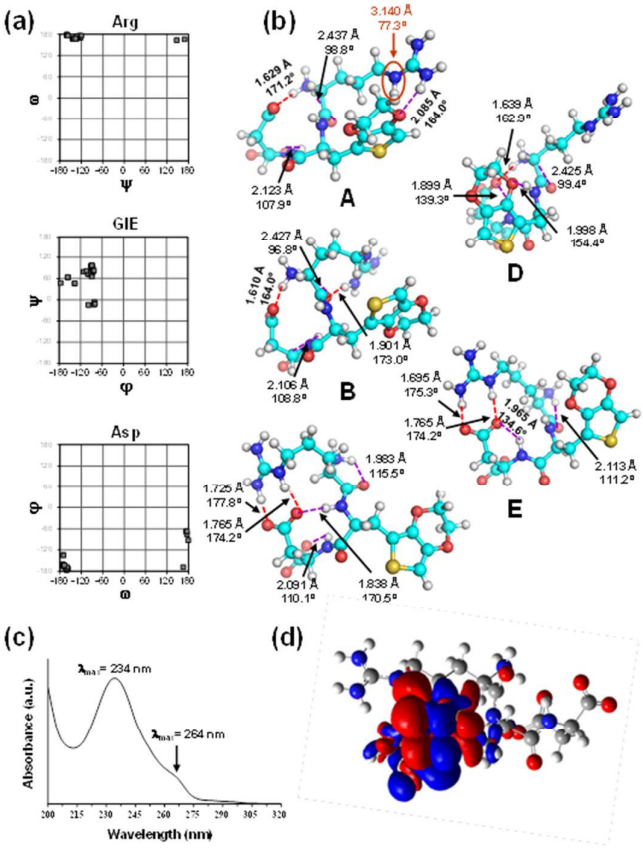

Figure 7. (a) Conformational maps constructed considering the backbone dihedral angles of the maps Arg (ω,ψ), GlE (φ,ψ) and Asp (ω,φ) residues, using the 25 unique minimum energy conformations identified in the clustering analysis for RG^ED. (b) Representation of the five low-energy structures (labeled from A to E in increasing order of energy) found in the clustering analysis for RG^ED/B in PBS. Salt bridges and hydrogen bonds are indicated by red and violet dashed lines, respectively. The red circle in A indicates that the N–H group involved in the N–H···π interaction with the thiophene group. Distances and angles associated to each of these interactions are given in Å and degrees, respectively. (c) UV-vis spectrum recorded for acetonitrile dilute RG^ED solution (37 μM). (d) Electronic density difference (excited – ground) corresponding to the first electronic transition ($\lambda^{(1)}_{max}$). Blue (red) regions indicate an increase (decrease) of electron density upon electronic transition.

The most characteristic interaction in the next minimum (C), with ΔE= 1.5 kcal/mol, corresponds to a double sc-sc salt bridge between the guanidium and carboxylate groups of Arg and Asp, respectively. As a consequence of such interaction, charged side groups are less exposed to the solvent in C than in A and B. This conformer also presents b-b interactions between the charged ammonium-end group and the amide of Arg as well as between the carboxylate-end group and the amide of Asp. In minimum D (ΔE= 3.9 kcal/mol) the Arg side chain adopts a fully extended arrangement that precludes the participation of the guanidium group in the formation of sc-sc and sc-b intramolecular interactions. Thus, interactions

observed in D are similar to those described for A-C. Finally, minimum E, with ΔE= 4.7 kcal/mol, exhibits a double sc-sc salt bridge between Arg and Asp as well as two sc-b interactions involving the charged end groups. These are similar to the interactions identified for C.

Results displayed in Figure 7b indicate that, in general, the overall shape of the unique minimum energy conformations with ΔE < 5 kcal/mol is appropriate to form intermolecular interactions with the integrin receptor. Thus, the general shape adopted by these conformations can be simply described as a small and deformed hairpin with the charged groups pointing outwards. As PEDOT chains are connected to RG^ED through the side group of the GlE residue, all these conformations are not expected to be affected by the formation of the conjugate. Accordingly, the functionality of the RGD adhesive sequence is expected to the preserved in the peptide of PEDOT-RG^ED conjugates.

While EDOT absorption spectrum exhibits a broad peak characterized by a double hump (264 nm and 255 nm), the spectrum of RG^ED in similar conditions (diluted in acetonitrile solution) exhibits a clear transition maximum appears at 234 nm with a small shoulder at 264 nm (see Figure 7c). In a previous work[24] on EDOT, we showed the importance of accounting for several conformations of such flexible structure to reproduce the experimental data with computational means. In the same vein, optical properties were here simulated in acetonitrile for A-E conformations starting from the five above-mentioned structures. All conformations present similar spectra with two close maximum absorption wavelengths ($\lambda^{(1)}_{max}$ and $\lambda^{(2)}_{max}$) at 234 nm and 232 nm (associated oscillator strengths > 0.1). No significant variation was observed when selecting one conformation or another. Looking at the electronic density difference of these transitions of A conformation, it is crystal clear that the electronic transition occurs on the G^E moiety and is therefore not affected by Arg and Asp flexibility (Figure 7d, see Figure S6 for similar plots for B-D). Comparing the computational results with experiment, the computed peak at 234 nm reproduces the experimental main peak while the observed experimental shoulder at 264 nm could not be resolved using such methodology. The shoulder is therefore not the result of conformational effects but is related to the fine structure of G^E.

Monitoring the influence of RG^ED in cell adhesion

The effect of the peptide in cell adhesion was evaluated by considering two epithelial (Vero and Saos-2) and two fibroblast (Cos-7 and MRC-5) cell lines. Vero and Cos-7 are cell lines derived from monkey kidney, while the origin of Saos-2 and MRC-5 was human bone and human lung, respectively. Quantitative results for cell adhesion assays are displayed in Figure 8a. These are expressed per area of substrate material and relative to those of the tissue culture polystyrene (TCPS), which was used as a control material. The number of cells adhered to the surface of PEDOT-RG^ED is significantly higher than that of PEDOT and TCPS for all cell lines, evidencing cell-specific adhesion promoted via RG^ED ligands conjugated to the PEDOT chains. The RGD peptide has been recognized as a molecular activator of the integrin cell surface receptor, which can induce intracellular signaling pathways.[39-41] This ability is preserved in RG^ED, where the Gly of RGD has been replaced by GlE. Especially, the activation of the integrin receptor through the interactions with the RG^ED peptide in the initial cell attachment step seems to affect subsequent cell spreading and survival through cell signaling molecules, such as focal adhesion kinase (FAK), as proposed for RGD.[40] Although this behavior is remarkable for the two conjugates, it is considerably more evident for PEDOT-RG^ED/B than for PEDOT-RG^ED/A. This has been attributed to the benefits produced by the synthetic strategy B in the properties of the resulting conjugate (*i.e.* enhancement of the roughness, wettability and electroactivity). In general, the relative viability of Saos-2 and MRC-5 human cell lines are higher favored than that of Vero and Cos-7 monkey kidney cell lines, independently of the substrate surface.

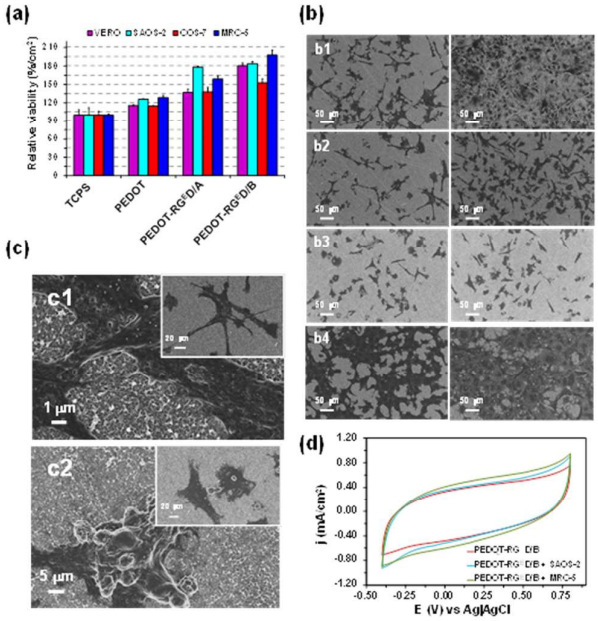

Figure 8. (a) Cellular adhesion on the surface of PEDOT, PEDOT-RG^ED/A and PEDOT-RG^ED/B. TCPS was used as a control substrate. Vero, Saos-2, Cos-7 and MRC-5 cells were cultured during 24 h. The experiments were performed using six samples for each substrate. (b) Adhesion of Vero, Saos-2, Cos-7 and MRC-5 cells (b1-b4) onto PEDOT-RG^ED/B. SEM micrographs reflect the homogeneous cell spreading. (c) High and low (inset) magnification SEM micrographs of Saos-2 and Cos-7 cells (c1 and c2, respectively) attached to PEDOT-RG^ED/B. (d) Control voltammograms in PBS of PEDOT-RG^ED/B uncoated and coated with Saos-2 and MRC-5 cells.

Figure 8b, which displays low magnification SEM micrographs of cells cultured onto both PEDOT-RG^ED/A and PEDOT-RG^ED/B, reveals not only the high density of adhered cells but also their homogeneous spreading onto the surface of the two conjugate films. Details about the adhesion of MRC-5 and Saos-2 cells onto the surface of PEDOT-RG^ED/B are provided in Figure 8c. As it can be seen, the cellular mechanism operating for the adhesion of the cells onto the conjugate films is the connection to the surface with filopodia. Thus, spreading of

the cells is achieved through an intimate contact between cells and the surface of the films.

On the other hand, the particular electrochemical properties of PEDOT, which exhibits higher cell viability than inert TCPS, also contribute to the superior cell attachment of PEDOT-RG^{E}D. Thus, the ability of this ECP to exchange ions with the cell through the cellular membrane is known to favor the formation of cell-surface interactions.[42] In order to evaluate the influence of cultured cells in the electrochemical activity of the conjugates, PEDOT-RG^{E}D/A and PEDOT-RG^{E}D/B films coated with cell monolayers were investigated by CV in PBS. Figure 8d compares the control voltammograms recorded for PEDOT-RG^{E}D/B coated with Saos-2 and MRC-5 cells with that obtained for the uncovered material (results obtained for PEDOT-RG^{E}D/A samples coated with are displayed in Figure S7). Cells do not affect the profile of the voltammograms, even though they provoke an enhancement of both the anodic current density at the reversal potential and of the electroactivity, which reflect the electrobioactivity of the prepared conjugates. Thus, cell monolayers increase the mobility of ions at the interfaces, the electroactivity increasing by about 10-25% with respect to the uncoated conjugates. According to these results, adhered cells promote the exchange of ions at the conjugate–cell interface rather than block the channels that allow the access and escape of ions.

Conclusions

The RG^{E}D peptide, which is an analogue of the adhesive RGD sequence, has been designed by chemical similarity with PEDOT and, subsequently, prepared through chemical synthesis. After this, PEDOT-RG^{E}D has been obtained by anodic polymerization, the EDOT side group of the GlE residue acting as a linker between the peptide and the polymer. Two different strategies have been used to produce materials with different surface roughness, wettability and electrochemical activity. Control onto these properties has been found to modulate the behavior of PEDOT-RG^{E}D conjugates as soft bioelectroactive supports for cell attachment.

Because the cell recognition abilities of the RGD motif remain in the RG^{E}D sequence, cell attachment and spreading on PEDOT-RG^{E}D have been significantly promoted with respect to PEDOT. Furthermore, the electrochemical activity of the ECP is preserved in the conjugate because both the small size of the peptide and the utilization of an EDOT ring as linker between the ECP and the peptide, do not affect the transport of charge. Indeed, the electrochemical activity of the conjugates increases upon the adhesion of cell monolayers. The successful design and controlled preparation of effective ECP-peptide conjugates open new and varied possibilities within the biomedical field. For example, the fabrication of multifunctional biomedical platforms for regenerative medicine, combining the presence the RG^{E}D adhesive sequence with other functional peptides in the same platform, and the development of artificial skin based on ECPs that, in addition, promote the regeneration of natural skin.[43]

Experimental section

Chemical characterization of RG^{E}D

Melting points were determined on a Gallenkamp apparatus and are uncorrected. IR spectra were registered on a Nicolet Avatar 360 FTIR spectrophotometer; ν_{max} is given for the main absorption bands. ^{1}H and ^{13}C NMR spectra were recorded on a Bruker AV-500, AV–400, ARX–300 or Varian Gemini 300 instrument at room temperature unless otherwise indicated, using the residual solvent signal as the internal standard, chemical shifts (δ) are expressed in ppm and coupling constants (*J*) in Hertz. High-resolution mass spectra were obtained on a Bruker Microtof-Q spectrometer.

Synthesis of PEDOT-RG^{E}D

Steps 1 and 2 of the synthetic process described in the text were carried out in a standard three electrode cell of 50 mL using steel AISI 316 sheets of 4 cm^2 area (surface roughness determined by atomic force microscopy: 11.4 nm) as working and counter electrodes. The reference electrode was an Ag|AgCl electrode containing a KCl saturated aqueous solution (E^0 = 0.222 V at 25ºC). The preparation of PEDOT and PEDOT-(protected RG^{E}D) films was performed by CA using a constant potential of 1.40 and 1.37 V, respectively. In all cases cells were filled with 50 mL of the corresponding acetonitrile solution. All electropolymerizations and cyclic voltammetry assays were conducted on a PGSTAT302N AUTOLAB potenciostat–galvanostat (Ecochimie, The Netherlands) equipped with the ECD module, which was connected to a PC computer controlled through the NOVA 1.6 software.

Characterization

The ESI provides details of the equipment and conditions used for characterization by contact profilometry, FTIR spectroscopy, X-ray photoelectron spectroscopy (XPS), standard ion chromatography, scanning electron microscopy (SEM), atomic force microscopy (AFM), contact angle measurements, cyclic voltammetry and UV-vis spectroscopy.

Conformation classification and clustering analysis

The procedure used to explore the potential energy hypersurface of the RG^{E}D peptide is described in the ESI. The list of unique minimum energy conformations was generated by comparing each of the 552 minimized structures among themselves. First, the list of minimized conformations was organized by rank ordering all them in an increasing energy. Unique minimum energy conformations were identified based on φ and ψ dihedral angles, which characterize the peptide backbone conformation and on hydrogen-bond and salt-bridge interactions. Four dihedral angles were defined for the whole peptide: ψ for Arg, φ and ψ for GlE and φ for Asp. The existence of interactions was accepted on the basis of the following geometric criterion: (a) for salt bridges, the distance between the centers of the interacting groups is shorter than 4.50 Å; (b) for hydrogen bonds, the H···O distance is shorter than 2.50 Å. Two structures were considered different when

differing in at least one of their dihedral angles by more than 60° or in at least one of the above interactions. All the structures classified as different were subsequently clustered based on salt bridges and hydrogen bonds.

Cell adhesion

Cos-7 (African green monkey kidney fibroblast cell line), Vero (African green monkey kidney epithelial cell line), MRC-5 (Human fetal lung fibroblast cell line) and Saos-2 (Human sarcoma osteogenic epithelial cell line) cells were cultured in Dulbecco's modified Eagle medium (DMEM) supplemented with 10% fetal bovine serum, 1% penicillin/streptomycin and 2 mM L-glutamine at 37ºC in a humidified atmosphere of 5% CO_2 in air. The cultured media were changed every two days. For sub-culture, cell monolayers were rinsed with PBS and detached by incubating them with 0.25% trypsin/EDTA for 5 min at 37ºC. Concentrations of cells were determined by counting at the Neubauer camera using 4% trypan blue as dye vital.

PEDOT and PEDOT-RG^{E}D films deposited onto steel AISI 316 sheets of 1 cm^2 were placed in plates of 24 wells and sterilized using UV irradiation for 15 min in a laminar flux cabinet. An aliquot of 0.5 mL containing 5×10^4 cells was deposited on the substrate of each well. The plate was incubated under culture conditions for 60 min to promote the cell attachment to the film surface. Finally, 1 mL of the culture medium was added to each well. Controls of adhesion were simultaneously performed by culturing cells on the surface of the tissue culture polystyrene (TCPS) plates. Cell adhesion was evaluated after 24 hours of culture using the MTT [3-(4,5-dimethylthiazol-2-yl)-2,5-diphenyltetrazolium bromide] assay, which determines the cell viability.[44] This assay measures the ability of the mitochondrial dehydrogenase enzyme of viable cells to cleave the tetrazolium rings of the MTT and form formazan crystals, which are impermeable to cell membranes and, therefore, are accumulated in healthy cells. This process is detected by a colour change: the characteristic pale yellow of MTT transforms into the dark blue of formazan crystals. The viability results were normalized to TCPS control as relative percentages.

Results were derived from the average of four replicates (n= 4) for each independent experiment. ANOVA and Turkey tests were performed to determine the statistical significance, which was considered at a confidence level of 95% ($p < 0.05$).
Before the carbon coating for examination by SEM, samples covered with cells were fixed in a 2.5% glutaraldehyde PBS solution overnight at 4ºC. Then, they were dehydrated by washing in ethanol battery (30º, 50º, 70º, 90º, 95º and 100º) at 4ºC for 30 minutes per wash. Finally, samples were air-dried, and sputter-coated with carbon before SEM observation.

Acknowledgements

Authors are in debt to supports from MINECO and FEDER (MAT2012-34498, and CTQ2013-40855-R), Generalitat de Catalunya (XRQTC), CESCA and Gobierno de Aragón-FSE (research group E40). D.J. is indebted to the European Research Council (ERC) for support in the framework of the ERC StG grant Marches 278845.

Notes and references

1 E. Ruoslahti and M. D. Pierschbacher, *Science*, 1987, **238**, 491–497.
2 M. D. Pierschbacher and E. Ruoslahti, *Nature*, **309**, 30–33.
3 R. O. Hynes, *Cell*, 1992, **69**, 11–25.
4 G. Cheng, V. Castelletto, R. R. Jones, C. J. Connon and I. W. Hamley, 2011, 1326–1333.
5 A. Li, A. Hokugo, A. Yalom, E. J. Berns, N. Stephanopoulos, M. T. McClendon, L. A. Segovia, I. Spigelman, S. I. Stupp and R. Jarrahy, *Biomaterials*, 2014, **35**, 8780–8790.
6 K. Fukunaga, H. Tsutsumi and H. Mihara, *Biopolymers*, 2013, **100**, 731–737.
7 K. M. Galler, L. Aulisa, K. R. Regan, R. N. D'Souza and J. D. Hartgerink, *J. Am. Chem. Soc.*, 2010, **132**, 3217–3223.
8 E. S. Gil, B. B. Mandal, S.-H. Park, J. K. Marchant, F. G. Omenetto and D. L. Kaplan, *Biomaterials*, 2010, **31**, 8953–8963.
9 J. Wu, J. Rnjak-Kovacina, Y. Du, M. L. Funderburgh, D. L. Kaplan and J. L. Funderburgh, *Biomaterials*, 2014, **35**, 3744–3755.
10 B. J. Kim, Y. S. Choi and H. J. Cha, *Angew. Chem. Int. Ed.*, 2012, **51**, 675–678.
11 T. J. Dennes, G. C. Hunt, J. E. Schwarzbauer and J. Schwartz, *J. Am. Chem. Soc.*, 2007, **129**, 93–97.
12 G. Oyman, C. Geyik, R. Ayranci, M. Ak, D. Odaci Demirkol, S. Timur and H. Coskunol, *RSC Adv.*, 2014, **4**, 53411–53418.
13 V. Castelletto, R. J. Gouveia, C. J. Connon and I. W. Hamley, *Eur. Polym. J.*, 2013, **49**, 2961–2967.
14 P. Viswanathan, E. Themistou, K. Ngamkham, G. C. Reilly, S. P. Armes and G. Battaglia, *Biomacromolecules*, 2015, **16**, 66–75.
15 Z. Yang, S. Yuan, B. Liang, Y. Liu, C. Choong and S. O. Pehkonen, *Macromol. Biosci.*, 2014, **14**, 1299–1311.
16 G. M. Whitesides, *Small*, 2005, **1**, 172–179.
17 S. Zhang, *Nat. Biotechnol.*, 2003, **21**, 1171–1178.
18 T.-Y. Liu, W. M. Hussein, Z. Jia, Z. M. Ziora, N. A. J. McMillan, M. J. Monteiro, I. Toth and M. Skwarczynski, *Biomacromolecules*, 2013, **14**, 2798–2806.
19 M. Morell and J. Puiggalí, *Polymers*, 2013, **5**, 188–224.
20 H.-A. Klok, A. Rösler, G. Götz, E. Mena-Osteritz and P. Bäuerle, *Org. Biomol. Chem.*, 2004, **2**, 3541–3544.
21 E. De Giglio, L. Sabbatini and P. G. Zambonin, *J. Biomater. Sci. Polym. Ed.*, 1999, **10**, 845–858.
22 E. De Giglio, L. Sabbatini, S. Colucci and G. Zambonin, *J. Biomater. Sci. Polym. Ed.*, 2000, **11**, 1073–1083.
23 G. Fabregat, G. Ballano, E. Armelin, L. J. del Valle, C. Cativiela and C. Alemán, *Polym. Chem.*, 2013, **4**, 1412–1424.
24 G. Fabregat, G. Ballano, J. Casanovas, A. D. Laurent, E. Armelin, L. J. del Valle, C. Cativiela, D. Jacquemin and C. Alemán, *RSC Adv.*, 2013, **3**, 21069–21083.
25 L. Groenendaal, G. Zotti, P.-H. Aubert, S. M. Waybright and J. R. Reynolds, *Adv. Mater.*, 2003, **15**, 855–879.
26 L. Groenendaal, F. Jonas, D. Freitag, H. Pielartzik and J. R. Reynolds, *Adv. Mater.*, 2000, **12**, 481–494.
27 S. Kirchmeyer and K. Reuter, *J. Mater. Chem.*, 2005, **15**, 2077–2088.
28 S. Maione, G. Fabregat, L. J. Del Valle, G. Ballano, C. Cativiela and C. Alemán, *J. Pept. Sci.*, 2014, **20**, 537–546.
29 V. Castelletto, C. M. Moulton, G. Cheng, I. W. Hamley, M. R. Hicks, A. Rodger, D. E. López-Pérez, G. Revilla-López and C. Alemán, *Soft Matter*, 2011, **7**, 11405–11415.

30 G. Fabregat, B. Teixeira-Dias, L. J. del Valle, E. Armelin, F. Estrany and C. Alemán, *ACS Appl. Mater. Interfaces*, 2014, **6**, 11940–11954.
31 S. A. Spanninga, D. C. Martin and Z. Chen, *J. Phys. Chem. C*, 2010, **114**, 14992–14997.
32 D. Bhattacharyya and K. K. Gleason, *Chem. Mater.*, 2011, **23**, 2600–2605.
33 J. S. Stevens, A. C. de Luca, M. Pelendritis, G. Terenghi, S. Downes and S. L. M. Schroeder, *Surf. Interface Anal.*, 2013, **45**, 1238–1246.
34 N. Sakmeche, S. Aeiyach, J.-J. Aaron, M. Jouini, J. C. Lacroix and P.-C. Lacaze, *Langmuir*, 1999, **15**, 2566–2574.
35 J. Chastain, *Handbook of X-ray Photoelectron Spectroscopy: A Reference Book of Standard Spectra for Identification and Interpretation of XPS Data*, Eden Prairie, MN: Perkin-Elmer, 1992.
36 G. Zotti, S. Zecchin, G. Schiavon, F. Louwet, L. Groenendaal, X. Crispin, W. Osikowicz, W. Salaneck and M. Fahlman, *Macromolecules*, 2003, **36**, 3337–3344.
37 D. Aradilla, F. Estrany, E. Armelin and C. Alemán, *Thin Solid Films*, 2010, **518**, 4203–4210.
38 K. D. Gibson and H. A. Scheraga, *J. Comput. Chem.*, 1987, **8**, 826–834.
39 E. Ruoslahti, *Annu. Rev. Cell Dev. Biol.*, 1996, **12**, 697–715.
40 F. G. Giancotti, *Science*, 1999, **285**, 1028–1033.
41 R. O. Hynes, *Cell*, 2002, **110**, 673–687.
42 L. J. del Valle, F. Estrany, E. Armelin, R. Oliver and C. Alemán, *Macromol. Biosci.*, 2008, **8**, 1144–1151.
43 T. F. Otero, J. G. Martínez and J. Arias-Pardilla, *Electrochim. Acta*, 2012, **84**, 112-128.
44 T. Mosmann, *J. Immunol. Methods*, 1983, **65**, 55–63.